SAND2019-0714C

Engineered Barrier Material Interactions at Elevated Temperatures: Bentonite-Metal Interactions Under Elevated Temperature Conditions

Carlos F. Jové Colón[a], Florie A. Caporuscio[b], Kirsten Sauer[c], and Michael C. Cheshire[d]

[a] cfjovec@sandia.gov. Sandia National Laboratories, Nuclear Waste Disposal Research and Analysis Department, P.O Box 5800 MS-0779, Albuquerque, New Mexico, 87185 USA.
[b] floriec@lanl.gov. Los Alamos National Laboratories, Earth and Environmental Sciences Division, SM-30 Bikini Atoll Rd., Los Alamos, New Mexico, 87545 USA.
[c] sauer@lanl.gov. Los Alamos National Laboratories, Earth and Environmental Sciences Division, SM-30 Bikini Atoll Rd., Los Alamos, New Mexico, 87545 USA.
[d] cheshiremc@ornl.gov. Oak Ridge National Laboratories, Oak Ridge, Tennessee, 37831 USA.

The development of deep repository concepts in the USA is evaluating generic options for disposal of heat-generating nuclear spent nuclear fuel (SNF) waste for a suite of host rock media (clay rock, granite, salt). Large waste canister designs (e.g., dual purpose canisters or DPC's) are currently being considered to accommodate many SNF assemblies. Large amounts of SNF in the waste packages will produce high thermal loads generating temperatures in excess of 200 °C for long periods of time. For a bentonite backfilled repository concept, prolonged exposure to high temperatures will induce chemical reactions in the engineered barrier system (EBS), particularly at barrier interfaces. Our focus is on experimental investigations and the application of thermodynamic modeling to evaluate clay-zeolite phase equilibria as a function of temperature and fluid chemistry. Experimental work on barrier material interactions under hydrothermal conditions (150 – 300 °C, 15-16 MPa) has elucidated mineral phase changes in Wyoming (Colony mine) bentonite in the presence of steel phases. Glassy material in bentonite is replaced by analcime-wairakite phases, and through apparent clinoptilolite recrystallization. The initial increase in dissolved silica leads to authigenic quartz formation. Such mineral assemblage suggests an initially silica-rich environment (analcime, clinoptilolite) moving towards Si-depleted conditions. Analcime-wairakite compositions suggest a well-defined solid-solution between these Na and Ca end-members. Smectite clay in these experiments is stable with Fe-saponite and chlorite growth co-existing with binary/ternary sulfides at steel interfaces. Little or no illite was observed in the reaction products which could be tied to silica oversaturation and low K in the system. The thermodynamic analysis is used to evaluate thermodynamic data and develop phase diagrams to describe stability field relations of secondary mineral phase occurrences. This analysis allows for delineation of potential reaction pathways in bentonite clay degradation and interactions with metallic phases. One example of this is the important role of dissolved silica plus other phase components to the formation of alteration mineralogy observed in these interactions. All these investigations are key to the assessment of thermally-induced degradation zones in the EBS during the thermal period and their effect on barrier performance in the safety assessment.

I. Introduction

Permanent disposition of spent nuclear fuel (SNF) in various geologic environments (clay rock, granite, salt) has motivated the evaluation of generic disposal concepts in the USA [1]. The most commonly-accepted concept of high-level nuclear waste disposal is the deep underground emplacement of steel waste-filled canisters with a bentonite barrier backfill between waste package and host rock. Fig. 1 shows a schematic representation of the engineered barrier system (EBS) for longitudinal emplacement of waste canisters in clay rock. The analysis EBS design concepts to isolate heat-generating waste canisters is key to the long-term (i.e., hundreds to tens of thousands of years) safety and isolation performance of the repository. An important aspect of this analysis is the nature of chemical interactions with EBS interfaces and the natural barrier (host rock) at elevated temperatures and pressures. For example, one potential disposal concept for SNF is to use high capacity dual purpose canisters (DPCs) emplaced with bentonite barrier material in the subsurface repository [2, 3]. DPCs are waste canister that can accommodate up to 37 SNF pressurized water reactor (PWR) assemblies and are expected to generate enough radionuclide decay heat to drive temperatures in excess of 200°C at the canister surface [2]. Therefore, such elevated temperatures will affect the bentonite/canister interface and other barrier backfill materials surrounding the waste package. In general, DPCs are made from steel or stainless-steel materials [3].

Long-term repository performance and safety strongly depends on barrier integrity under a wide range of environmental conditions (e.g., elevated temperatures and pressures, radioactivity). The effect of high temperature exposure in the presence of aqueous fluids produces surface metal corrosion of the canister and

Sandia National Laboratories is a multimission laboratory managed and operated by National Technology & Engineering Solutions of Sandia, LLC, a wholly owned subsidiary of Honeywell International Inc., for the U.S. Department of Energy's National Nuclear Security Administration under contract DE-NA0003525.

mineralogic alteration and/or phase transformations in the bentonite backfill material. Therefore, experimental work to improve our understanding of clay barrier interactions and thermal-hydrological-mechanical-chemical (THMC) couplings at high temperatures are key to evaluate thermal effects from waste decay heat and the extent of sacrificial zones in the EBS. Moreover, experimental and modeling investigations have provided key information central to the assessment of thermal limits and the implementation of the reference case to evaluate EBS configuration and the repository layout (e.g., thermal loads, drift spacing).

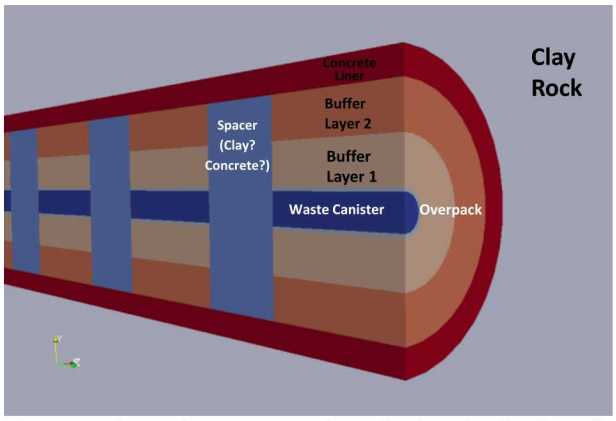

Fig. 1. Schematic representation of a longitudinal section of a backfilled single drift with multiple waste canisters and a multi-layered EBS [4].

The focus of this communication is to present results from past and ongoing investigations on barrier material interactions that involve experimental and modeling studies related to deep subsurface disposition of nuclear waste in geologic environments.

I.A. Background

I.A.1. Experimental Methods

To investigate the effects of high temperatures on the barrier material interactions, a series of hydrothermal experiments between bentonite and metallic phases (steels, copper) were conducted at temperatures ranging from 150 to 300 °C (ramped and isothermal) and pressures of 15-16 MPa [5-7]. Also, experiments in the presence of bentonite plus Opalinus Clay rock and corresponding starting solutions were also conducted but the presented results will focus on bentonite-only experiments. These experiments allow for the analysis of pre-run and *post-mortem* material in the characterization of altered and newly-formed phases particularly at barrier material interfaces. This information is used in the evaluation of chemical reactions between bentonite and metallic phases. The bentonite used in the experiments was obtained from a reducing horizon in Colony, Wyoming. This bentonite contains primarily Na-bearing montmorillonite with minor amounts of clinoptilolite and lesser plagioclase, biotite, calcite, and sulfide minerals (e.g., pyrite). The bentonite material was crushed and sieved to a size of < 3 mm and used with a free moisture content of ~15.5 wt. %. The synthetic solution used in the experiments has the composition of a deep groundwater in crystalline basement rock (Stripa sample V2, 69-4) [8]. This solution was then filtered through a 0.45 µm filter and sparged with He before each experiment. The salt solution was added at 9:1 water:bentonite ratio. Reactants were loaded into a flexible gold cell and fixed into a 500 mL gasket confined closure reactor [9]. As noted previously, experiments in the presence of bentonite plus Opalinus Clay rock and corresponding starting solutions were also conducted but overall results on the main reaction products are similar both types of experiments. Any differences in the experimental results when using Opalinus Clay rock and associated solution as starting material will be noted in the discussion.

TABLE I. Synthetic groundwater chemistry Stripa sample V2 (69-4), Frape et al. 2003) used in the experiments.

Species	Concentration (mg/L)
Ca^{2+}	89
Cl^{-}	1045
K^{+}	583
Na^{+}	167
Si	1
SO_4^{2-}	47
Sr^{2+}	0.05
TDS	1934
pH	8.59

Experiments were pressurized to 150 - 160 bars and were heated isothermally at temperatures of 150 to 300°C (depending on the experiment) for several weeks. Reaction liquids were extracted during the experiments and analyzed to investigate the aqueous geochemical evolution in relationship to mineralogical alterations. The sampled reaction liquids were split three-ways producing aliquots for unfiltered anion, unfiltered cation, and filtered (0.45 µm syringe filter) cation determination. All aliquots were stored in a refrigerator at 1°C until analysis. Pre-run and post-experiment solids retrieved from the experiment were characterized using X-ray diffraction (XRD) and scanning electron microscopy with energy dispersive X-ray spectroscopy (SEM/EDS). Chemical analysis of collected solutions (major cations and trace metals) were performed using inductively coupled plasma-optical emission spectrometry (ICP-OES) and inductively coupled plasma-mass spectrometry (ICP-MS) utilizing EPA methods. Inorganic anion samples were analyzed by ion chromatography (IC).

I.B. Results and Discussion

I.B.1. Steel/Copper – Bentonite Interactions

Stainless steel (304SS and 316SS) corrosion products associated with bentonite interactions produces four layers onto the steel substrate (1) chromite-like ($FeCr_2O_4$) passivation layer in contact with unaltered stainless steel, (2) Si-Cl-S mixed phases, (3) discrete pentlandite ($(Ni,Fe)_9S_8$) and millerite (NiS), and (4) an Fe-saponite $[M_{0.33}(Fe,Mg)_3(Si_{3.67}Al_{0.33})O_{10}(OH)_2]$ outer layer with occasional minor chlorite (Fig. 2). This layered oxide structure is consistent with observations of 316L alloy corrosion under PWR conditions (i.e., 325°C, 155 bar) [10-12]. Post-experiment characterization of stainless steel reaction products shows uniform corrosion at the temperature conditions of the experiments. Occurrence of surface Fe-bearing clay associated with corrosion products also show a close relationship with chlorite. However, there was no significant alteration to the montmorillonite phase at distance from the metal interface (> 1 mm from metal surface). Minor formation of pentlandite ($(Ni,Fe)_9S_8$) and millerite (NiS) sulfides developed at the early stages of corrosion. The formation of these sulfides is likely due to pyrite (FeS_2) degradation in bentonite and their occurrence is closely associated with the Fe-saponite phase on the stainless-steel substrates. Formation of Fe-saponite is related to the close interaction of Fe-bearing and Si-rich fluids due to stainless steel leaching and bentonite dissolution.

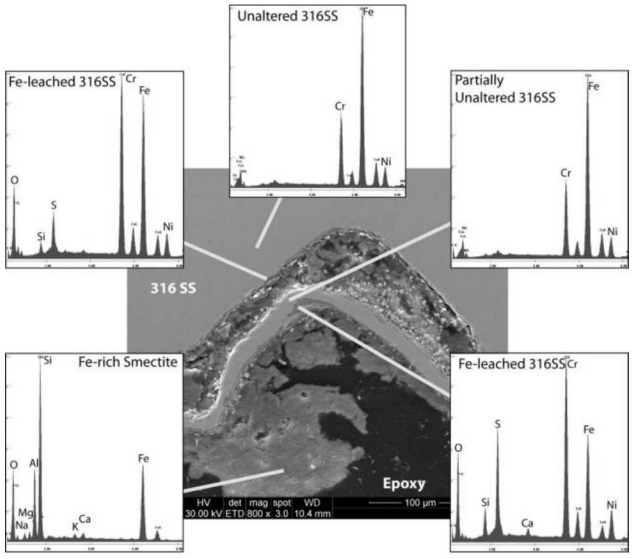

Fig. 2. SEM image showing a cross-section of 316SS run product depicting Fe-saponite/chlorite growth. Chemical analyses of 316SS and interface run products show significant Fe leaching from the steel surface and formation of a Cr-rich outer layer [4, 6].

Low carbon steel degradation produces three layers of corrosion products on the stainless steel substrate (1) magnetite-like (Fe_3O_4) layer onto the steel surface, (2) pyrrhotite (Fe_7S_8), and (3) an Fe-saponite $[M_{0.33}(Fe,Mg)_3(Si_{3.67}Al_{0.33})O_{10}(OH)_2]$ outer layer (Fig. 3). The magnetite-like oxide layer observed at the steel-bentonite interface show no apparent formation of a passivation layer and no indication of corrosion hindrance. Interface textures show pitting corrosion with development of Fe-rich smectite coating with structures suggesting growth perpendicular to the steel substrate. Pyrrhotite (Fe_7S_8) platelets formed alongside the smectite phases (Fig. 3). The Fe-saponite overall morphology indicates a precipitation mechanism instead of a solid-state transformation.

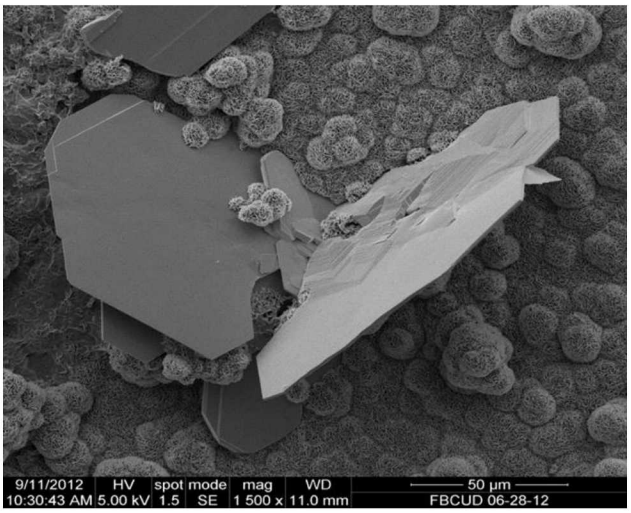

Fig. 3. SEM image of pyrrhotite nested in bed of botryoidal Fe-saponite on a substrate of low carbon steel [6].

The primary copper corrosion mechanism associated with bentonite interaction is sulfide-induced (sulfide attack) corrosion to produce chalcocite (Cu_2S; Fig. 4). As observed in the figure, the chalcocite layer grows over the corroded/pitted copper surface. The occurrence of chalcocite is characterized by its hexagonal morphology forming discrete plates to fully coalesced patches on the copper surface. Chalcocite crystallization on the copper surface is the result of surface crystallization from solution via sequestration of dissolved sulfur species (e.g., H_2S, HS^-) from pyrite decomposition in the bentonite under hydrothermal conditions. Other Cu-bearing phases observed in the post-experiment characterization are minor covellite (CuS) and atacamite. The latter is believed to form from late-stage uptake of Cl from the synthetic brine.

I.B.2. Bentonite Clay Alteration and Zeolite Formation

As described earlier, the bentonite material used in the experiments contains mainly Na-montmorillonite with minor amounts of clinoptilolite, feldspars, biotite, cristobalite, quartz, and pyrite. The Na-montmorillonite texture shows the characteristic foily or 'cornflake' morphology often associated with smectite grains. The Na-montmorillonite has the structural composition $(Na_{.31},Ca_{.04},K_{.01})(Al_{1.53},Fe_{.21},Mg_{.18},Ti_{.01})(Si_{3.98},Al_{.02})O_{10}(OH)_2$ [5, 13].

Clinoptilolite textures in the bentonite seems to preserve the precursor volcanic glass shard morphology with a structural composition of $(Na_{4.30},Ca_{0.39},K_{0.14},Mg_{0.20})(Si_{29.82},Al_{6.28},Fe_{0.03})O_{72}{\cdot}nH_2O$ (n ~ 21, clinoptilolite stoichiometric basis).

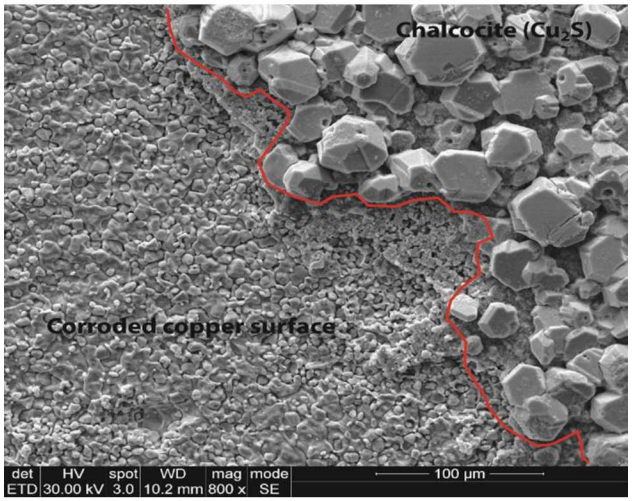

Fig. 4. Post-experiment SEM image of corroded copper surface (lower left) and the secondary chalcocite surface growth (upper right) [7, 9].

Feldspar phases are mainly represented by albitic plagioclases and K-feldspar. Pyrite in bentonite shows framboidal and cubic morphologies [5]. XRD data of samples from ramped temperatures and isothermal experiments are hard to differentiate suggesting that illite-smectite was not produced in the course of the experiment. The clinoptilolite in the bentonite starting material transforms to analcime at higher temperatures, releasing SiO_2 and water. Analcime forms as 5 – 10 µm anhedral to subhedral trapezohedrons (Fig. 5). Anhedral analcime crystallized initially as an agglomeration of nano-sized, spherical crystals followed by coarsening of analcime to subhedral, trapezohedral analcime. The Si/Al ratio tend to be low (i.e., 2.83) in the early stages of analcime formation relative to a value of 2.97 in the subhedral analcime [9]. It should be noted that experiments involving bentonite only as the starting silicate phase only produces analcime. However, starting material mixtures of Opalinus Clay and bentonite produces an intermediate analcime-wairakite composition at higher temperatures. The occurrence of this compositional join highlights the importance of zeolite solid solutions in the stability of secondary mineral assemblages within the thermal regime between diagenetic and low-grade metamorphic systems [12]. Fig. 6 shows the wairakite-analcime solid solution trend based on zeolite compositions obtained from the experiments and those from the literature [14-17]. The clinoptilolite compositions are also plotted in Fig. 6 for comparison. It shows that the Si/Al ratio of clinoptilolite and/or relic glass material in bentonite can release silica during their dissolution to stabilize analcime.

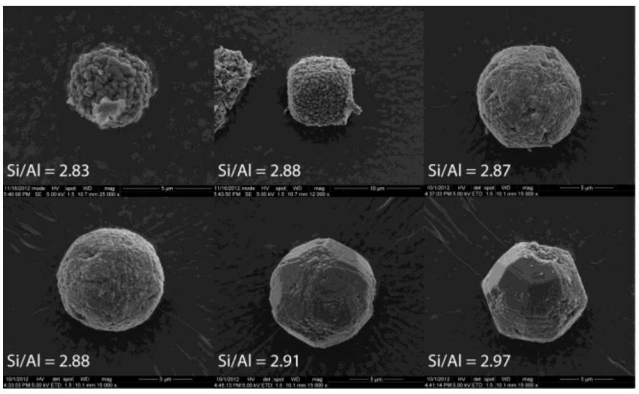

Fig. 5. Analcime growth stages associated with a systematic Si/Al changes. Anhedral analcime formed early as an agglomeration of nano-sized, spherical crystals followed by ripening of analcime crystals to subhedral, trapezohedral analcime [13].

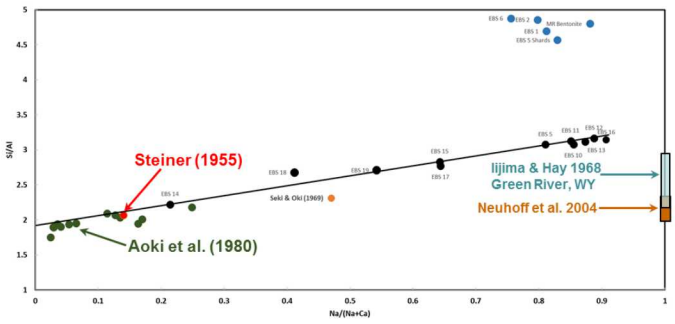

Fig. 6. Graph of Si/Al ratio versus zeolite composition for analcime-wairakite join. Data points represented by filled black circles are the experimental data. Data points in blue (upper left) are experimental data for either glass shard or clinoptilolite samples. Data points on analcime-wairakite compositions from other authors are shown for comparison (color labeled according to the data source). The black trend line is a guide for the eye [12].

Illite is precluded from forming in the bentonite-only experiments and is linked to silica oversaturation along with low K bulk content in solution. The occurrence of wairakite in the Opalinus Clay experiments at 300°C is probably linked to abundant Ca in the aqueous phase and high temperatures. These observations indicate the importance of $SiO_{2(aq)}$ activity in determining the zeolite stable assemblage and the absence of illite which is stable at low $SiO_{2(aq)}$ activities. Fig. 7 shows the stability relations of saponite, analcime, and wairakite as the alteration mineral assemblage relative to the smectite clay phase as a function of $SiO_{2(aq)}$ activity and temperature. Phase boundaries in this diagram would change slightly according to the activities of mineral components in the aqueous phase within the chosen phase composition and corresponding thermodynamic data. Nevertheless, the overall topological representation of the stable mineral assemblage in this diagram is consistent with experimental observations and the occurrence of clay-zeolite phases at elevated temperatures.

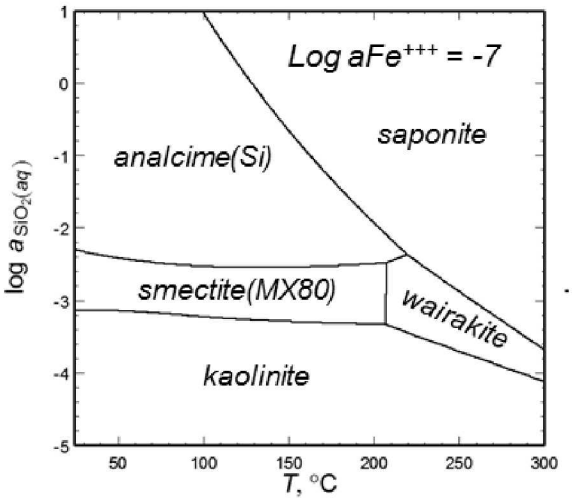

Fig. 7. Activity phase diagram of $SiO_{2(aq)}$ vs. temperature for clay-zeolite equilibria. Notice wairakite stabilization with increasing temperature at low $SiO_{2(aq)}$ activities relative to saponite and analcime (see text) [12].

The diagram in Fig. 7 was constructed using thermodynamic data from multiple sources [17-28]. The thermodynamic evaluation of this system is part of ongoing work reconciling experimental observations with equilibria between minerals and the aqueous phase.

II. CONCLUSIONS

Hydrothermal experiments between bentonite and metallic phases (steels, copper) and bentonite plus Opalinus Clay rock were conducted up to temperatures of 300°C and 15-16 MPa. Fe-saponite forms at the bentonite-steel interface along with Fe and Cu sulfide phases for steel and copper starting material, respectively. Pyrite decomposition in the bentonite produces sulfur towards the formation of these phases. Clinoptilolite in the starting bentonite transforms to Si-rich analcime at high temperatures. Zeolite compositions shows the development of an analcime-wairakite solid solution in experiments with Opalinus Clay rock where higher amounts of Ca may have contributed to this compositional join. Illite is precluded from forming under Si-rich conditions as observed from post-experiment mineral characterization and thermodynamic evaluation of phase equilibria. Steel corrosion in the presence of bentonite produces a chromite-like ($FeCr_2O_4$) passivation layer in contact with unaltered stainless steel and a magnetite-like phase for low-carbon steel. Copper corrosion associated with bentonite interactions produces chalcocite (Cu_2S) growth along over the corroded/pitted surface.

$SiO_{2(aq)}$ activity plus other system components are key to the alteration mineralogy observed in these barrier interaction experiments. Analcime is the product of clinoptilolite alteration to produce $SiO_{2(aq)}$. The occurrence of Fe-bearing saponite plus zeolite highlights the importance of $SiO_{2(aq)}$ and other aqueous species in determining the alteration mineral assemblage at elevated temperatures. This study provides important information to the design and performance of the EBS and clay barrier degradation at interfaces under elevated temperatures. Such conditions are anticipated for scenarios involving large canisters containing heat-generating nuclear waste for disposal in deep geological repository environments.

ACKNOWLEDGMENTS

The authors acknowledge our gratitude to Yifeng Wang (SNL), Ed Matteo (SNL), Kevin McMahon (SNL), Emily Stein (SNL), William Spezialetti (DOE NE), Prasad Nair (DOE NE), Mark Tynan (DOE NE), and Tim Gunther (DOE NE) for their helpful discussions and contributions on various topics covered in this work. Sandia National Laboratories is a multi-mission laboratory managed and operated by National Technology and Engineering Solutions of Sandia, LLC., a wholly owned subsidiary of Honeywell International, Inc., for the U.S. Department of Energy's National Nuclear Security Administration under contract DE-NA-0003525.

REFERENCES

1. Nutt, M., M. Voegele, C. Jove-Colon, Y. Wang, R. Howard, J. Blink, H.-H. Liu, E. Hardin, and K. Jenni, *Used Fuel Disposition Campaign Disposal Research and Development Roadmap (Fuel Cycle Research and Development)*, 2011. p. 1-138.
2. Greenberg, H.R., J. Wen, and T. Buscheck, *Scoping Thermal Analysis of Alternative Dual-Purpose Canister Disposal Concepts (LLNL-TR-639869)*,

2013, Lawrence Livermore National Laboratory: Livermore, CA. p. 54.
3. Hardin, E., D. Clayton, R.L. Howard, J.M. Scaglione, E. Pierce, K. Banerjee, M. Voegele, H.R. Greenberg, J. Wen, T. Buscheck, J.T. Carter, and T. Severynse, *Preliminary Report on Dual-Purpose Canister Disposal Alternatives (FCRD-UFD-2013-000171)*, U.F.D.C. U.S. Department of Energy, Fuel Cycle Technologies, Editor 2013, Sandia National Laboratories: Albuquerque, NM USA.
4. Jové Colón, C.F., J.A. Greathouse, S. Teich-McGoldrick, R.T. Cygan, P.F. Weck, G.A. Hansen, L.J. Criscenti, F.A. Caporuscio, M. Cheshire, M.S. Rearick, M.K. McCarney, H.R. Greenberg, T.J. Wolery, M. Sutton, M. Zavarin, A.B. Kersting, J.B. Begg, J.A. Blink, T. Buscheck, A. Benedicto-Cordoba, P. Zhao, J. Rutqvist, C.I. Steefel, J. Birkholzer, H.-H. Liu, J.A. Davis, R. Tinnacher, I. Bourg, L. Zheng, and V. Vilarrasa, *EBS Model Development and Evaluation Report (FCRD-UFD-2013-000312)*, 2013, Sandia National Laboratories, SAND2013-8512 P: Albuquerque, NM. p. 508.
5. Cheshire, M., F.A. Caporuscio, M.S. Rearick, C.F. Jové Colón, and M.K. McCarney, *Bentonite evolution at elevated pressures and temperatures: An experimental study for generic nuclear repository designs.* American Mineralogist, 2014. **99**: p. 1662-1675.
6. Cheshire, M.C., F.A. Caporuscio, C.F. Jové Colón, and K.E. Norskog, *Fe-saponite growth on low-carbon and stainless steel in hydrothermal-bentonite experiments.* Journal of Nuclear Materials, 2018. **511**: p. 353-366.
7. Caporuscio, F.A., S.E.M. Palaich, M.C. Cheshire, and C.F. Jové Colón, *Corrosion of copper and authigenic sulfide mineral growth in hydrothermal bentonite experiments.* Journal of Nuclear Materials, 2017. **485**: p. 137-146.
8. Zanonato, P.L., P. Di Bernardo, and I. Grenthe, *A calorimetric study of the hydrolysis and peroxide complex formation of the uranyl(VI) ion.* Dalton Trans, 2014. **43**(6): p. 2378-83.
9. Jové Colón, C.F., P.F. Weck, K. Kuhlman, L. Zheng, J. Rutqvist, K. Kim, J. Houseworth, F.A. Caporuscio, M. Cheshire, S. Palaich, K.E. Norskog, M. Zavarin, T.J. Wolery, J.L. Jerden, J.M. Copple, T. Cruse, and W.L. Ebert, *Evaluation of Used Fuel Disposition in Clay-Bearing Rock (Vol. I) (FCRD-UFD-2015-000124)*, 2015, Sandia National Laboratories: Albuquerque, NM. SAND2015-7827 R.
10. Terachi, T., T. Yamada, T. Miyamoto, K. Arioka, and K. Fukuya, *Corrosion behavior of stainless steels in simulated PWR primary water—Effect of chromium content in alloys and dissolved hydrogen—.* Journal of nuclear science and technology, 2008. **45**(10): p. 975-984.
11. Soulas, R., M. Cheynet, E. Rauch, T. Neisius, L. Legras, C. Domain, and Y. Brechet, *TEM investigations of the oxide layers formed on a 316L alloy in simulated PWR environment.* Journal of Materials Science, 2013. **48**(7): p. 2861-2871.
12. Jové Colón, C.F., Y. Wang, T. Hadgu, L. Zheng, J. Rutqvist, H. Xu, K. Kim, M. Voltolini, X. Cao, P.M. Fox, P.S. Nico, F.A. Caporuscio, K.E. Norskog, M. Zavarin, T.J. Wolery, C. Atkins-Duffin, J.L. Jerden, V.K. Gattu, and W.L. Ebert, *Evaluation of Used Fuel Disposition in Clay-Bearing Rock (SFWD-SFWST-2017-000006)*, 2017, Sandia National Laboratories: Albuquerque, NM. SAND2017-10533 R. p. 442.
13. Jové Colón, C.F., P.F. Weck, D.C. Sassani, L. Zheng, J. Rutqvist, C.I. Steefel, K. Kim, S. Nakagawa, J. Houseworth, J. Birkholzer, F.A. Caporuscio, M. Cheshire, M.S. Rearick, M.K. McCarney, M. Zavarin, A. Benedicto-Cordoba, A.B. Kersting, M. Sutton, J.L. Jerden, K.E. Frey, J.M. Copple, and W.L. Ebert, *Evaluation of Used Fuel Disposition in Clay-Bearing Rock (FCRD-UFD-2014-000056)*, 2014, Sandia National Laboratories, SAND2014-18303 R: Albuquerque, NM. p. 434.
14. Aoki, M. and H. Minato, *Lattice constants of wairakite as a function of chemical composition.* American Mineralogist, 1980. **65**(11-12): p. 1212-1216.
15. Iijima, A. and R. Hay, *Analcime composition in tuffs of Green River Formation of Wyoming.* American Mineralogist, 1968. **53**(1-2): p. 184-&.
16. Seki, Y. and Y. Oki, *Wairakite-analcime solid solutions from low-grade metamorphic rocks of the Tanzawa Mountains, Central Japan.* Mineralogical Journal, 1969. **6**(1-2): p. 36-45.
17. Neuhoff, P.S., G.L. Hovis, G. Balassone, and J.F. Stebbins, *Thermodynamic properties of analcime solid solutions.* American Journal of Science, 2004. **304**(1): p. 21-66.
18. Helgeson, H.C., J.M. Delany, H.W. Nesbitt, and D.K. Bird, *Summary and Critique of the Thermodynamic Properties of Rock-Forming Minerals.* American Journal of Science, 1978. **278**: p. 1-229.
19. Kiseleva, I., A. Navrotsky, I.A. Belitsky, and B.A. Fursenko, *Thermochemistry and phase equilibria in calcium zeolites.* American Mineralogist, 1996. **81**(5-6): p. 658-667.
20. Blanc, P., P. Piantone, A. Lassin, and A. Burnol, *Thermochimie: Sélection de constantes thermodynamiques pour les éléments majeurs, le plomb et le cadmium*, in *Rapport final BRGM/RP-54902-FR* 2006, BRGM: France. p. 1-157.
21. Blanc, P., A. Lassin, P. Piantone, M. Azaroual, N. Jacquemet, A. Fabbri, and A. Gaucher, *Thermoddem: A geochemical database focused on low temperature water/rock interactions and waste materials.* Applied Geochemistry, 2012. **27**: p. 2107-2116.

22. Blanc, P., P. Vieillard, H. Gailhanou, S. Gaboreau, É. Gaucher, C.I. Fialips, B. Madé, and E. Giffaut, *A generalized model for predicting the thermodynamic properties of clay minerals.* American Journal of Science, 2015. **315**(8): p. 734-780.
23. Gailhanou, H., J.C. van Miltenburg, J. Rogez, J. Olives, M. Amouric, E.C. Gaucher, and P. Blanc, *Thermodynamic properties of anhydrous smectite MX-80, illite IMt-2 and mixed-layer illite-smectite ISCz-1 as determined by calorimetric methods. Part I: Heat capacities, heat contents and entropies.* Geochimica et Cosmochimica Acta, 2007. **71**(22): p. 5463-5473.
24. Gailhanou, H., P. Blanc, J. Rogez, G. Mikaelian, H. Kawaji, J. Olives, M. Amouric, R. Denoyel, S. Bourrelly, V. Montouillout, P. Vieillard, C.I. Fialips, N. Michau, and E.C. Gaucher, *Thermodynamic properties of illite, smectite and beidellite by calorimetric methods: Enthalpies of formation, heat capacities, entropies and Gibbs free energies of formation.* Geochimica et Cosmochimica Acta, 2012. **89**: p. 279-301.
25. Gailhanou, H., P. Blanc, J. Rogez, G. Mikaelian, K. Horiuchi, Y. Yamamura, K. Saito, H. Kawaji, F. Warmont, and J.-M. Grenèche, *Thermodynamic properties of saponite, nontronite, and vermiculite derived from calorimetric measurements.* American Mineralogist, 2013. **98**(10): p. 1834-1847.
26. Holland, T.J.B. and R. Powell, *An improved and extended internally consistent thermodynamic dataset for phases of petrological interest, involving a new equation of state for solids.* Journal of Metamorphic Geology, 2011. **29**: p. 333-383.
27. Rimstidt, J.D., *Quartz solubility at low temperatures.* Geochimica et Cosmochimica Acta, 1997. **61**(13): p. 2553-2558.
28. Tutolo, B.M., X.-Z. Kong, W.E. Seyfried, Jr., and M.O. Saar, *Internal consistency in aqueous geochemical data revisited: Applications to the aluminum system.* Geochimica et Cosmochimica Acta, 2014. **133**: p. 216-234.